agronomy

MDPI

Article

Vertical Profiles of Solar-Induced Chlorophyll Fluorescence and Their Relationship with Canopy Gross Primary Productivity in Wheat

Jie Zhu, Rui Huang *, Xinwen Xu, Yujuan Huang, Wei Li, Yangyang Gu, Leilei Liu, Hengbiao Zheng, Chongya Jiang, Tao Cheng, Yongchao Tian, Yan Zhu, Weixing Cao and Xia Yao *

National Engineering and Technology Center for Information Agriculture, Key Laboratory of Crop System Analysis and Decision Making, Ministry of Agriculture and Rural Affairs, Jiangsu Key Laboratory for Information Agriculture, Nanjing Agricultural University, 1 Weigang Road, Nanjing 210095, China
* Correspondence: huangrui@njau.edu.cn (R.H.); yaoxia@njau.edu.cn (X.Y.)

Abstract

The accurate estimation of wheat productivity is important for food security assessment. However, how vertical variation in canopy structure and physiology affects solar-induced chlorophyll fluorescence (SIF) and its relationship with gross primary productivity (GPP) remains unclear. To address this gap, this study estimated near-infrared SIF (SIF_{NIR}) emissions from three wheat leaf layers using fluorescence yield, LAI, and APAR, quantified their contributions to canopy SIF, and assessed the effects of vertical heterogeneity. SIF–GPP relationships were examined using diurnal measurements at anthesis and grain filling. All three leaf layers exhibited seasonal SIF_{NIR} patterns consistent with those of canopy SIF. The first leaf layer contributed the largest proportion of total canopy SIF_{NIR}, reaching 63.51%, and showed the strongest relationship with total canopy SIF_{NIR} ($R^2 = 0.83$). The sum of SIF_{NIR} emissions from the three layers ($SIF_{NIR_L1+L2+L3}$) was also strongly related to total near-infrared SIF at the photosystem level (SIF_{NIR_tot}; $R^2 = 0.84$). Omitting vertical variation in either LAI or $SIFy_{NIR}$ affected canopy SIF_{NIR_tot}, with LAI having the greater influence. SIF_{NIR} from all three layers was strongly associated with canopy GPP, with R^2 values of 0.83, 0.87, and 0.79 for the first, second, and third layers, respectively. The second layer SIF_{NIR_L2} and the three-layer sum $SIF_{NIR_L1+L2+L3}$ explained the same proportion of variation in GPP ($R^2 = 0.87$), exceeding that explained by SIF_{NIR_tot} ($R^2 = 0.81$). These findings improve our understanding of how vertical canopy heterogeneity influences SIF emissions in wheat and highlight the importance of SIF from the middle leaf layer for estimating canopy GPP.

Keywords: wheat; solar-induced chlorophyll fluorescence; vertical canopy heterogeneity; gross primary productivity; agricultural remote sensing

Check for updates

Academic Editor: Xujun Ye

Received: 15 October 2026
Revised: 10 November 2026
Accepted: 16 November 2026
Published: 18 November 2026

Copyright: © 2026 by the authors. Licensee MDPI, Basel, Switzerland. This article is an open access article distributed under the terms and conditions of the Creative Commons Attribution (CC BY) license.

1. Introduction

Wheat is a major staple crop cultivated extensively worldwide [1]. Accurate estimation and prediction of wheat photosynthetic productivity are therefore important for supporting global food security and informing carbon budget assessments. Solar-induced chlorophyll fluorescence (SIF) has been shown to be an effective indicator of gross primary productivity (GPP) in wheat [2–5].

Although SIF can provide reliable estimates of vegetation productivity, the relationship between SIF and productivity is sensitive to complex structural and physiological factors

within vegetation canopies [6–9]. Crop canopies also exhibit vertical heterogeneity. Previous studies have shown that both chlorophyll a and b (Cab) and leaf area index (LAI) vary from the top to the bottom of wheat canopies [10–13]. Leaf Cab content directly affects SIF emission yield (SIFy) and photosynthetic efficiency [14,15]. It is also closely related to the capacity of leaves to absorb photosynthetically active radiation (PAR) and influences the amount of PAR intercepted by different canopy layers [16], thereby contributing to differences in SIF emissions among leaf layers at different heights. LAI governs the photosynthetic area of vegetation, while its vertical distribution influences PAR interception by leaves in different canopy layers, thereby affecting SIF emissions and photosynthesis. Furthermore, the vertical distributions of LAI and Cab influence the transmission of optical signals within the canopy [17]. Mutual shading among leaf layers leads to differences in their contributions to the observed SIF signal. Taken together, vertical canopy heterogeneity affects both vegetation SIF emissions and photosynthetic productivity.

Previous studies have investigated the effects of vertical canopy heterogeneity on canopy SIF emissions. For example, using SCOPE simulations and field measurements, Yang et al. [18] showed that vertical heterogeneity in leaf physiological and biochemical properties markedly affects top-of-canopy reflectance, fluorescence, and photosynthesis, highlighting the importance of accounting for this heterogeneity when predicting these variables. Using a modified version of the FluorFLIGHT radiative transfer model (RTM), Hornero et al. [19] demonstrated that understory SIF contributions should be considered when quantifying SIF within heterogeneous forest crowns and canopies from aggregated pixels. Regaieg et al. [20] and Gao et al. [21] also found that non-photosynthetic woody components strongly affect SIF emissions and emphasized the influence of understory vegetation on top-of-canopy SIF. However, few studies have quantified the contributions of individual wheat leaf layers to total canopy SIF. Furthermore, few studies have compared the effects of vertical variation in canopy structure (LAI) and physiology (SIFy) on canopy SIF in wheat. Quantifying and understanding these effects is therefore important for simulating SIF signals and disentangling their structural and physiological controls.

Vegetation photosynthetic productivity results from photosynthesis throughout the canopy, whereas SIF signals are measured externally. This mismatch may reduce the accuracy of SIF-based productivity estimates. To address this issue, several algorithms have been developed to calculate total near-infrared SIF emission at the photosystem level (SIF_{NIR_tot}; [22–24]). However, these calculations still rely on SIF observations acquired from above the canopy. Morozumi et al. [25] investigated how SIF from upper, middle, and lower forest layers responded to seasonal variation in GPP. They found that calculated SIF_{NIR_tot} was proportional to the sum of SIF emissions from the individual layers and that lower-layer SIF tracked seasonal GPP variation before leaf emergence in the upper canopy. Using field measurements and model simulations of SIF and GPP across forest layers, Zhu et al. [26] quantified the contributions of individual layers to canopy SIF. SIF_{NIR_tot} was more strongly correlated with GPP than observed SIF, and near-infrared SIF (SIF_{NIR}) summed across layers also showed a stronger correlation with GPP than observed SIF_{NIR}. Cab, leaf inclination angle, LAI, and senescent material in the corresponding canopy layers were the dominant controls on reflectance and SIF signals observed at the canopy top and in the understory. Previous studies have focused primarily on forests. For wheat, however, few studies have yet examined how SIF from individual leaf layers responds to canopy GPP or whether SIF summed across layers improves GPP estimation compared with observed canopy SIF and calculated SIF_{NIR_tot}. Addressing these questions is important for understanding the relationship between SIF and GPP. The uppermost three leaves are important photosynthetic source leaves during reproductive development in wheat and rice, providing a physiological basis for focusing on these leaf positions [27,28]. Combining

leaf fluorescence yields with layer-specific LAI and APAR allows vertical SIF variation to be examined in terms of both physiological and structural differences. This study therefore extends previous work on vertical SIF distribution by linking individual wheat leaf layers to canopy fluorescence and GPP.

Specifically, this study aimed to: (1) quantify the contributions of SIF emitted by different wheat leaf layers to total canopy SIF; (2) compare the effects of vertical heterogeneity in canopy structure (LAI) and leaf physiology (SIFy) on canopy SIF emissions; (3) assess the responsiveness of SIF from different leaf layers to canopy GPP; and (4) determine whether SIF summed across the three leaf layers is more strongly associated with canopy GPP than calculated SIF_{NIR_tot}.

2. Materials and Methods

2.1. Experimental Design

This study was conducted from November 2017 to May 2018 at the experimental station of the National Engineering and Technology Center for Information Agriculture in Zhujiaqiao Village, Baipu Town, Rugao, Jiangsu Province, China. The region has a subtropical monsoon climate influenced by the East Asian monsoon, with a mean annual temperature of 15–16 °C, annual precipitation of 990–1060 mm, and approximately 120 rainy days per year. The soil at the experimental site has a loam texture. Each plot had an area of 30 m^2 (5 m × 6 m). The wheat cultivars were Shengxuan 6 (V1, compact plant type) and Yangmai 16 (V2, loose plant type). Wheat was sown in rows on 2 November at a planting density of 1.5×10^6 plants ha^{-1} under three nitrogen fertilizer rates (N0: 0 kg ha^{-1}; N1: 150 kg ha^{-1}; N2: 300 kg ha^{-1}). We collected leaf and canopy measurements from six plots, with one observed plot for each combination of two wheat cultivars and three nitrogen rates and no independent plot replication within combinations. These plots provided a range of canopy structural and physiological conditions for examining vertical SIF variation and its relationship with canopy GPP. Urea (46% N) was used as the nitrogen fertilizer and applied in a 1:1 ratio as basal fertilizer and topdressing at jointing. In addition, 120 kg ha^{-1} of phosphorus fertilizer (P_2O_5) and 135 kg ha^{-1} of potassium fertilizer (K_2O) were applied as basal fertilizers. Other management practices were the same as those used in local high-yielding wheat fields. Starting at flowering (flowering and grain-filling stages), transparent gas-exchange chambers were placed in the three plots V1N0, V1N1, and V1N2 to collect photosynthetic data.

2.2. Data Collection

To investigate the contributions of SIF emitted by different leaf layers to total canopy SIF, leaf and canopy data were collected from six plots at key growth stages. These included spectra and leaf area for leaves at different positions, together with canopy spectra and LAI. Diurnal measurements of canopy SIF and photosynthesis were also collected from V1N0, V1N1, and V1N2 at two key growth stages.

Measurements of leaves at different positions: Leaf spectra (Section 2.2.1) and leaf area were measured at tillering (day of year, DOY 67), jointing (DOY 81), booting (DOY 97), heading (DOY 106), anthesis (DOY 111), and grain filling (DOY 123). Measurements covered six plots comprising two cultivars and three nitrogen treatments (V1N0, V1N1, V1N2, V2N0, V2N1, and V2N2), designed to provide variation in canopy physiological and structural characteristics. All measurements were conducted on clear days between 10:00 and 14:00 local time (LT), as close as possible to the first clear day of each growth stage. Clear days were selected to reduce rapid changes in incoming sunlight caused by passing clouds and to obtain more stable illumination during spectral measurements. Three wheat plants were randomly selected in each plot, and the first (D1), second (D2), and

third (D3) leaves from the top were measured. These plants were treated as within-plot subsamples. Measurements were averaged separately for each leaf position to obtain one value per leaf position per plot. Individual plants were not treated as independent field replicates. Because the third leaf from the top was too small at tillering, D3 data were obtained only for V1N2 and V2N2 at this stage.

Canopy measurements: Canopy spectra were measured in the same six plots at the key growth stages corresponding to the leaf measurements (Section Canopy Spectral Measurements). Measurements were conducted on dates adjacent to the leaf measurement dates, under clear skies between 10:00 and 14:00 LT. In addition, diurnal spectral and photosynthetic data were collected from V1N0, V1N1, and V1N2 at anthesis and grain filling. Spectral measurements followed the canopy spectral measurement procedure, while photosynthetic measurements followed the method described in Section 2.2.2. Measurements were taken hourly from 08:00 to 16:00 LT. At grain filling, however, weather conditions limited data collection to 09:00, 11:00, 12:00, 14:00, 15:00, and 16:00 LT on a single clear day.

2.2.1. Leaf Data Collection

For D1, D2, and D3 leaves, SIF at 761 nm (SIF_{NIR}) was used to match the wavelength of the canopy SIF measurements. Leaf spectra were acquired using an ASD spectroradiometer (Analytical Spectral Devices, Boulder, CO, USA) coupled to a Fluowat leaf clamp (Producción por mecanizados Villanueva S.L.U., Almazora, Spain). Measurements covered 350–2500 nm and were taken approximately one-third of the leaf length from the base, avoiding the main vein. Sunlight entered the clamp at an angle of 45°, and an optical fiber collected the spectral signals. Reference-panel, leaf-reflected, and leaf-transmitted radiance were recorded. For fluorescence measurements, a 650-nm short-pass filter blocked incident radiation at wavelengths above 650 nm, allowing fluorescence emission to be measured.

Leaf area for D1, D2, and D3 leaves (LAD1, LAD2, and LAD3, respectively) was obtained using a leaf area meter (LI-3000, LI-COR Inc., Lincoln, NE, USA).

2.2.2. Canopy Data Collection

Canopy Spectral Measurements

Canopy spectra were measured using an ASD FieldSpec 4 Hi-Res spectroradiometer (Analytical Spectral Devices, Boulder, CO, USA) and a QE Pro spectrometer (Ocean Optics Inc., Dunedin, FL, USA). Both instruments acquired canopy radiance and reference-panel observations concurrently. The QE Pro spectra supported SIF retrieval, while the ASD spectra were used to derive reflectance and PAR. An L-shaped pole positioned the QE Pro optical fiber above the canopy. During acquisition, the ASD fiber tip was held immediately beside the QE Pro tip to obtain closely aligned viewing footprints. Both fibers faced downward from a height of 1 m above the wheat canopy, sampling an area approximately 0.4 m in diameter. Incoming solar irradiance was represented by radiance reflected from a calibrated Spectralon reference panel (Labsphere, Inc., North Sutton, NH, USA), whose reflectance was close to unity across 350–2500 nm. To stabilize the QE Pro signal, its detector was held at 25 °C. Measurements from both instruments underwent dark-current correction and integration-time optimization. Five scans were averaged for each observation to reduce noise.

Flux Measurements

A CAPTS-100 system (Shufeng Biological Technology Co., Ltd., Shanghai, China) was used to monitor CO_2 exchange and environmental conditions [29]. The system included transparent gas-exchange chambers, each measuring 1 m × 1 m × 1.5 m, a combined sensor for photon flux, temperature, and humidity, and a main unit equipped with CO_2 and H_2O

analyzers. Recorded variables included canopy net photosynthetic rate (Pn). Automatic observations continued throughout the day and night whenever rainfall was absent. Following chamber closure, the measurement interval was 2 min during daytime and 3 min at night. Observations were discarded if PPFD varied by more than 30%, expressed as the coefficient of variation, during the measurement interval. Nighttime observations provided canopy respiration rates (Rn). For each plot at each growth stage, a linear regression was fitted between Rn and the corresponding air temperature. The fitted relationship was then applied to daytime air temperatures from the same plot and growth stage to estimate daytime Rn. A similar linear temperature–respiration approach has been used in chamber measurements [30]. GPP was calculated by adding estimated daytime Rn to measured daytime Pn.

Canopy Structural and Biochemical Measurements

At each selected growth stage, 30–40 tillers were randomly sampled from each plot for laboratory measurements. The samples were cleaned and de-rooted before being separated into stems, leaves, and spikes. Their green leaf area was measured using the LI-3000 leaf area meter described in Section 2.2.1. Mean green leaf area per tiller was then combined with field tiller density to calculate canopy LAI. Tiller density was estimated from counts in two randomly selected row segments, each 1 m long.

2.3. Data Calculations

2.3.1. Calculation of Leaf SIF Parameters

Leaf reflectance and transmittance were derived from the radiance measurements of the reference panel and leaves. These values were then used to calculate the fraction of photosynthetically active radiation absorbed by leaves ($fAPAR_{Dn}$) over 400–700 nm.

$$fAPAR_{Dn}^{400–700} = \left(1 - R_{Dn}^{400–700} - TM_{Dn}^{400–700}\right) \quad (1)$$

where R_{Dn} and TM_{Dn} denote leaf reflectance and transmittance within this wavelength range, respectively.

Photosynthetically active radiation (PAR_{Dn}) was calculated from the incident reference-panel spectral radiance derived from reference-panel measurements:

$$PAR_{Dn} = \int_{\lambda=400}^{\lambda=700} I_{\lambda Dn} d\lambda \quad (2)$$

where I_λ denotes reference-panel spectral radiance at wavelength λ.

Leaf absorbed photosynthetically active radiation ($APAR_{Dn}$, $W/m^2/sr$) was calculated from PAR_{Dn} and $fAPAR_{Dn}$:

$$APAR_{Dn} = \int_{\lambda=400}^{\lambda=700} [I_{\lambda Dn} \times fAPAR_{Dn}] d\lambda \quad (3)$$

SIF emission at 761 nm in the near-infrared region (SIF_{NIR_Dn}, $mW/m^2/nm/sr$) was extracted and used to calculate leaf fluorescence yield ($SIFy_{\lambda_Dn}$, nm^{-1}). The factor of 1000 converts APAR from $W/m^2/sr$ to $mW/m^2/sr$:

$$SIFy_{NIR_Dn} = \frac{SIF_{NIR_Dn}}{APAR_{Dn} \times 1000} \quad (4)$$

Leaf fluorescence yields were calculated separately for D1, D2, and D3 and used to represent the SIF yields of the first, second, and third leaf layers, denoted as $SIFy_{NIRL1}$, $SIFy_{NIRL2}$ and $SIFy_{NIRL3}$ (nm^{-1}), respectively. Leaf absorptance, PAR, APAR, and SIF yield were calculated following the spectral approach described by Jia et al. [31].

2.3.2. Calculation of Canopy Vegetation Indices and Radiation Variables

Reflectance (R_{λ_C}) was calculated as the ratio of canopy radiance to reference-panel radiance (Köppl et al. [32], Equation (5)). APAR was also calculated from the ASD measurement. fAPARc denotes the fraction of photosynthetically active radiation absorbed by vegetation (Equation (8); [33]). PAR was calculated by integrating reference-panel radiance over 400–700 nm, and canopy APAR ($W/m^2/sr$) was obtained by multiplying PAR by canopy fAPAR (Equations (6) and (9); [34]).

$$R_{\lambda C} = \frac{L_{\boldsymbol{\lambda C}}}{I_{\boldsymbol{\lambda C}}} \quad (5)$$

$$PAR_C = \int_{\lambda=400}^{\lambda=700} I_{\lambda_C} d_\lambda \quad (6)$$

$$\text{Rededge NDVI}_C = \frac{R_{750_C} - R_{705_C}}{R_{750_C} + R_{705_C}} \quad (7)$$

$$\text{fAPARc} = 1.37 \times \text{Rededge NDVIc} - 0.17 \quad (8)$$

$$\text{APARc} = \text{PARc} \times \text{fAPARc} \quad (9)$$

where λ denotes wavelength, R_{λ_C} is the reflectance at wavelength λ, L_{λ_C} is the canopy radiance, and I_{λ_C} was approximated as the radiance measured from the reference panel. Numerical subscripts indicate wavelengths in nanometers.

2.3.3. Calculation of Canopy SIF Parameters

SIF intensity was retrieved from canopy radiance and irradiance spectra using the advanced fluorescence spectrum reconstruction method (aFSR) [35]. SIF values at 761 nm were calculated and denoted as SIF_{NIRc} ($mW/m^2/nm/sr$).

The SIF_{NIR} signal before canopy scattering and absorption was represented by total $SIF_{NIR_tot_C}$ ($mW/m^2/nm/sr$), estimated using the method proposed by Zeng et al. [24]. NIRv was calculated as the product of near-infrared reflectance and NDVI following Badgley et al [36] (Equation (12)). NDVI followed the normalized-difference formulation of Rouse et al. [37], using reflectance at 800 and 680 nm in this study (Equation (13)).

$$SIF_{NIR_tot_C} = \frac{SIF_{NIR_C}}{\text{fesc}} \quad (10)$$

$$\text{fesc} = \frac{NIR_{V_C}}{\text{fAPARc}} \quad (11)$$

$$NIR_{V_C} = R_{NIR_C} \times NDVI_C \quad (12)$$

$$NDVI_C = \frac{R_{800_C} - R_{680_C}}{R_{680_C} + R_{800_C}} \quad (13)$$

where fesc is the escape fraction of near-infrared SIF (SIF_{NIRC}), and R_{NIRC} denotes near-infrared reflectance, evaluated here at 761 nm.

$$SIF_{yNIR_tot_C} = \frac{SIF_{NIR_tot_C}}{APAR_C \times 1000} \quad (14)$$

The yield of $SIF_{NIR_tot_C}$ ($SIFy_{NIR_tot_C}$, nm^{-1}) was calculated as the ratio of $SIF_{NIR_tot_C}$ to $APAR_C$, following Yang et al. [34].

2.3.4. Leaf-to-Layer Scaling

The uppermost three leaves are important photosynthetic source leaves during reproductive development in wheat and rice, contributing to carbon assimilation and grain filling [27,28]. This physiological importance, together with the relatively small size of leaves below the third position and the onset of their senescence after booting in our study, motivated our focus on the upper three leaf positions. Accordingly, the wheat canopy was represented by three leaf layers, L1, L2, and L3, corresponding to the first (D1), second (D2), and third (D3) leaves from the top, respectively.

Using measured LAI and leaf-level $SIFy_{NIR_Dn}$ for the leaf positions corresponding to each layer, we applied a mechanistic model following Chang et al. [38] to calculate near-infrared SIF from the nth leaf layer (SIF_{NIR_Ln}, $mW/m^2/nm/sr$). Leaf-level fluorescence yield ($SIFy_{NIR_Dn}$) was calculated as the ratio of leaf SIF at 761 nm to leaf APAR, as described in Section 2.3.1. The measured areas of D1–D3 were used to determine their relative leaf area fractions, which were multiplied by canopy LAI to obtain layer-specific LAI. Layer APAR was subsequently estimated from incoming PAR, layer-specific LAI, and the light extinction coefficient using Equations (16)–(18). Following the scaling approach of Chang et al. [38], SIF from each leaf layer was then calculated using the corresponding fluorescence yield and layer APAR:

$$SIF_{NIR_Ln} = SIFy_{NIR_Ln} \times APAR_{Ln} \times 1000 \quad (15)$$

where $SIFy_{NIRLn}$ denotes the near-infrared SIF emission yield of the nth leaf layer (Ln), obtained from $SIFy_{NIR_Dn}$ calculated for the corresponding leaf position in Section 2.3.1. Because $SIFy_{NIR}$ is relatively insensitive to variations in light intensity [39], the effect of light intensity on $SIFy_{NIR}$ was not considered in the calculations.

$APAR_{Ln}$ ($W/m^2/sr$) denotes the photosynthetically active radiation absorbed by the nth leaf layer. Following Chang et al. [38], $APAR_L$ was calculated as the difference between PAR entering layer L and PAR reaching layer L + 1 (Equation (16)). The incoming PAR for the first layer was denoted as PAR_{in_L1}, and PAR reaching the second layer (PAR_{in_L2}) was calculated using Equation (17). This procedure was repeated for successive layers to obtain APAR for each layer. The extinction coefficient, k, was calculated using measured canopy LAI and APARc obtained in Section 2.3.2 (Equation (18)).

$$APAR_{Ln} = PAR_{in_Ln} - PAR_{in_L(n+1)} \quad (16)$$

$$PAR_{in_L(n+1)} = PAR_{in_Ln} \times e^{-k \cdot LAI_{Ln}} \quad (17)$$

$$k = -\frac{\ln\left(1 - \frac{APARc}{PAR_{in}}\right)}{LAIc} \quad (18)$$

The extinction coefficient k was calculated separately for each observation and assumed constant across the three leaf layers.

After calculating SIF_{NIR} emissions from each leaf layer, total canopy SIF ($SIF_{NIR_L1+L2+L3}$) was obtained by summing SIF_{NIR_L1}, SIF_{NIR_L2}, and SIF_{NIR_L3}. The fractional contribution of each layer was calculated as the ratio of its SIF_{NIR} emission (SIF_{NIR_Ln}) to $SIF_{NIR_L1+L2+L3}$.

Canopy SIF is primarily influenced by vegetation structural and physiological parameters. LAI is an important canopy structural factor affecting SIF, while SIFy represents the physiological component. We therefore assessed the effects of vertical variation in these parameters on canopy SIF by assigning uniform values of either LAI or SIFy across the three leaf layers. To examine the effect of vertical variation in LAI_{Ln}, the LAI of each layer was set to the mean LAI of the three layers. The resulting total canopy SIFNIR was denoted as $ALSIF_{NIR_L1+L2+L3}$. Similarly, to examine the effect of vertical variation in SIFy, each layer was assigned the mean $SIFy_{Ln}$ of the three layers, and the resulting total SIF_{NIR} was denoted as $AFSIF_{NIR_L1+L2+L3}$.

2.3.5. Data Analysis

Relationships between leaf-layer SIF, canopy SIF, and GPP were examined using ordinary least-squares linear regression with an intercept. R^2 was used to describe the strength of these relationships, while RMSE and RE were used to assess agreement between the three-layer SIF estimates and canopy SIF. Shaded bands in the regression plots represent 95% confidence intervals for the fitted mean response.

Differences between Pearson correlation coefficients sharing the same response variable were assessed using two-sided Williams tests [40], using a common set of complete observations within each comparison group. Results were expressed as $\Delta r = r(A, Y) - r(B, Y)$, where A and B denote the compared SIF indicators and Y denotes canopy SIF or GPP. Positive Δr values indicate a higher correlation coefficient for A. Asterisks in Figure A1 indicate unadjusted $p < 0.05$. Statistical calculations were performed in Python 3.12.7.

3. Results

3.1. Seasonal Variations in SIFy and SIF Across Leaf Layers

Figure 1 shows the changes in leaf-layer and canopy SIF parameters across wheat growth stages. Both near-infrared SIF yield ($SIFy_{NIR_Ln}$; Figure 1a) and SIF_{NIR} (Figure 1b) initially increased and subsequently decreased in all leaf layers. In the first layer, $SIFy_{NIR_L1}$ declined slightly at booting before reaching its maximum at heading. In the second and third layers, $SIFy_{NIR_L2}$ and $SIFy_{NIR_L3}$ increased markedly from tillering to booting and changed little between booting and heading, with slight decreases observed in some plots. $SIFy_{NIR_L1}$ exceeded $SIFy_{NIR_L2}$ at all stages except booting, when $SIFy_{NIR_L2}$ was the highest. Overall, $SIFy_{NIR_L2}$ was higher than $SIFy_{NIR_L3}$.

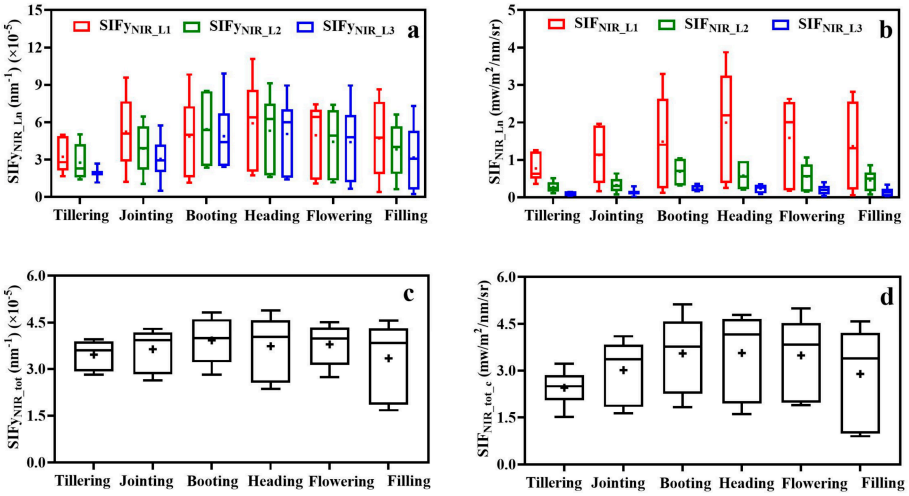


Figure 1. The variation trends of SIF in different leaf layers and canopy of wheat throughout the growing season: $SIFy_{NIR_Ln}$ in different leaf layers (**a**), SIF_{NIR_Ln} in different leaf layers (**b**), canopy $SIFy_{NIR_tot}$ (**c**), and canopy SIF_{NIR_tot} (**d**). Note: $SIFy_{NIR_Ln}$ was SIF yield at the near-infrared (NIR) for the nth leaf layer, SIF_{NIR_Ln} was SIF at the NIR for the nth leaf layer, $SIFy_{NIR_tot}$ was total near-infrared SIF yield at photosystem level, SIF_{NIR_tot} was total near-infrared SIF at photosystem level.

Differences among layers were more pronounced for SIF_{NIR} than for $SIFy_{NIR}$, with SIF_{NIR} consistently following the order L1 > L2 > L3. SIF_{NIR_L1} increased progressively from tillering to heading, peaked at heading, and then declined. In contrast, SIF_{NIR_L2} and SIF_{NIR_L3} peaked at booting and decreased thereafter.

At the canopy level, $SIFy_{NIR_tot}$ and SIF_{NIR_tot} followed patterns similar to those of the leaf-layer parameters, generally increasing and then decreasing, with relatively small changes between booting and heading (Figure 1c,d). Overall, the seasonal patterns of the second-layer SIF_{NIR} parameters most closely resembled those of the corresponding canopy parameters.

3.2. Contributions of SIFNIR from Different Wheat Leaf Layers to SIF_{NIR_tot}

Figure 2 shows the relationships between canopy SIF_{NIR_tot} and SIF_{NIR} from individual leaf layers and their three-layer sum. Summed SIF_{NIR} ($SIF_{NIR_L1+L2+L3}$) was strongly correlated with SIF_{NIR_tot} ($R^2 = 0.84$; Figure 2d), with a regression slope close to unity ($k = 0.895$). The corresponding RMSE and RE were 0.50 and 16.08%, respectively.

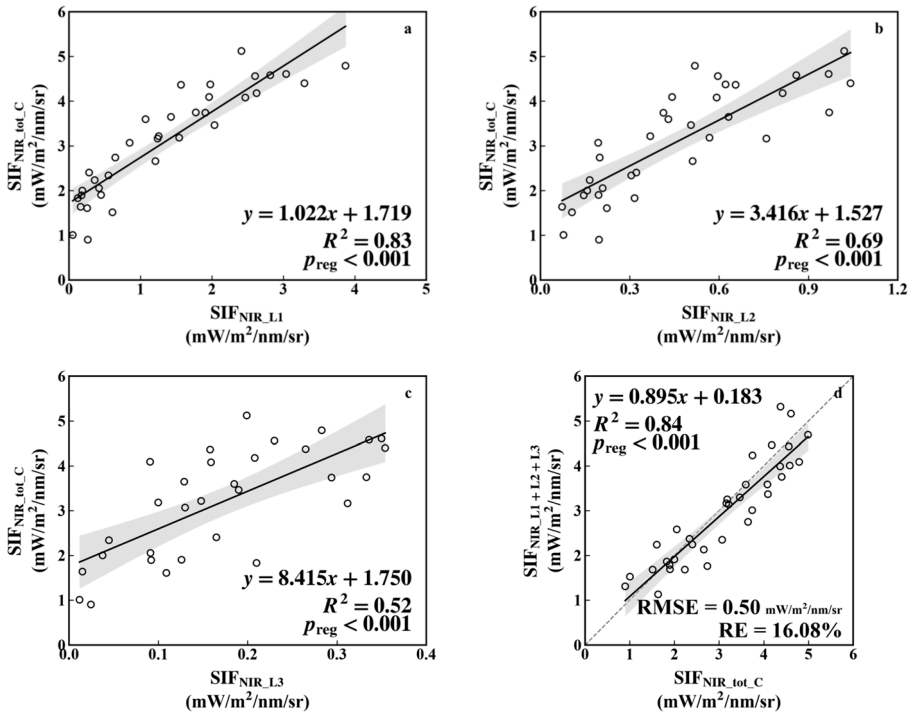


Figure 2. Scatter plot of $SIF_{NIR_L1+L2+L3}$ and SIF for different leaf layers against SIF_{NIR_tot} calculated from measured SIF_{NIR_C}: SIF_{NIR_L1} (**a**), SIF_{NIR_L2} (**b**), SIF_{NIR_L3} (**c**), and $SIF_{NIR_L1+L2+L3}$ (**d**).

To determine which leaf layer best represented canopy SIF, we examined the relationship between SIF_{NIR} from each layer and canopy SIF_{NIR_tot}. The first layer showed the strongest correlation ($R^2 = 0.83$; Figure 2a), closely matching that obtained for the three-layer sum. The second layer exhibited a weaker correlation ($R^2 = 0.69$; Figure 2b), while the third layer showed the weakest correlation ($R^2 = 0.52$; Figure 2c). The correlation with canopy SIF was significantly stronger for L1 than for L2 ($p = 0.0347$) and L3 ($p = 0.0041$). The difference between L2 and L3 was not significant ($p = 0.2764$; Figure A1a).

Table 1 presents the mean contributions of SIF emissions from individual leaf layers (SIF_{NIR_Ln}) to total canopy SIF ($SIF_{NIR_L1+L2+L3}$), while Figure 3 shows how these contributions varied across growth stages. The first layer accounted for the largest share of canopy SIFNIR, with a mean contribution of 63.51%, followed by L2 at 27.49%. L3 contributed the smallest share, averaging only 9%.

Table 1. The average proportion of SIF_{NIR_Ln} from different leaf layers to the total canopy $SIF_{NIR_L1+L2+L3}$.

Proportion of SIF from Different Leaf Layers to Total Canopy SIF			
Leaf layer	L1	L2	L3
Proportion (%)	63.51	27.49	9

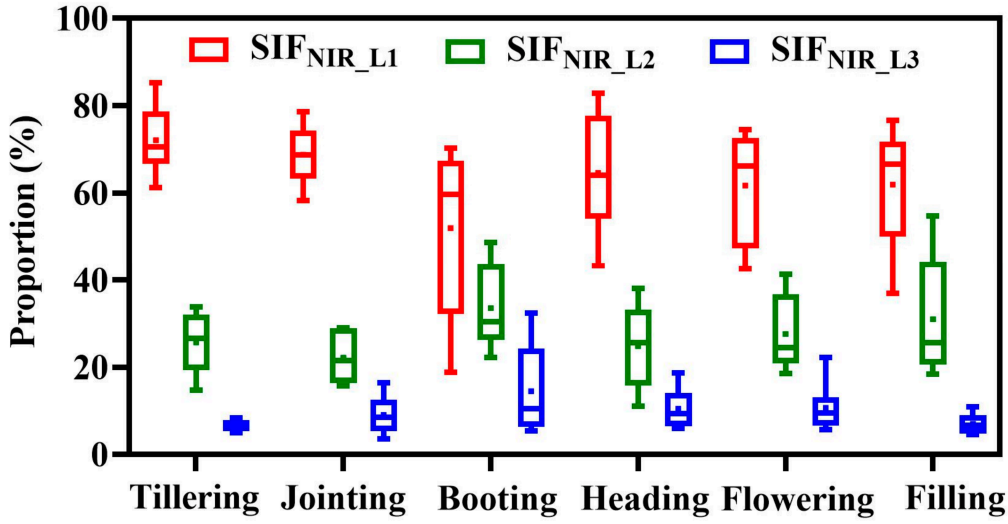


Figure 3. The proportion of SIF_{NIR} from each leaf layer to the total canopy SIF_{NIR} at different growth stages.

These proportions varied over the growing season. The contribution of SIF_{NIR_L1} generally decreased from tillering to grain filling, with a pronounced decline at booting, a recovery at heading, and a subsequent gradual decrease. The contribution of SIF_{NIR_L2} remained relatively stable overall, showing little variation among tillering, jointing, heading, and anthesis, but relatively higher values at booting and grain filling. The contribution of SIF_{NIR_L3} increased progressively up to booting and declined thereafter.

3.3. Effects of Vertical Canopy Distribution on Total SIF

To assess the effects of vertical variation in canopy physiological and structural parameters on canopy SIF, $AFSIF_{NIR_L1+L2+L3}$ and $ALSIF_{NIR_L1+L2+L3}$ were calculated by assigning uniform $SIFy_{NIR_Ln}$ or $LAI_{_Ln}$ values, respectively, across the three leaf layers. Their relationships with canopy SIF_{NIR_tot} are shown in Figure 4. For comparison, Figure 2d shows the relationship between $SIF_{NIR_tot_C}$ and $SIF_{NIR_L1+L2+L3}$ calculated with vertical variation in both parameters retained.

Although SIF_{NIR} from all three layers captured seasonal patterns of wheat growth (Figure 1a,b), neglecting vertical variation in $SIFy_{NIR_Ln}$ weakened the relationship between the calculated $AFSIF_{NIR_L1+L2+L3}$ and canopy SIF_{NIR_tot} ($R^2 = 0.81$; Figure 4a). RMSE and RE were 0.54 mW m^{-2} nm^{-1} sr^{-1} and 17.31%, respectively. Relative to the calculation retaining vertical variation in both parameters, R^2 decreased by 0.03, while RMSE and RE increased by 0.04 mW m^{-2} nm^{-1} sr^{-1} and 1.23 percentage points, respectively. Neglecting vertical variation in $LAI_{_Ln}$ had a greater effect: the relationship between $ALSIF_{NIR_L1+L2+L3}$ and $SIF_{NIR_tot_C}$ yielded an R^2 of 0.76, an RMSE of 0.64 mW m^{-2} nm^{-1} sr^{-1}, and an RE of 20.49% (Figure 4b). Compared with the calculation retaining vertical variation in both parameters, R^2 decreased by 0.08, while RMSE and RE increased by 0.14 mW m^{-2} nm^{-1} sr^{-1} and 4.41 percentage points, respectively.

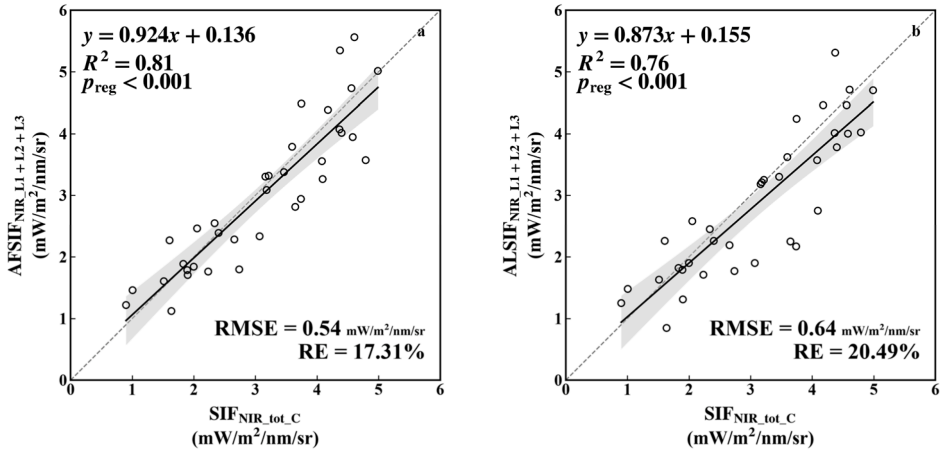


Figure 4. Scatter plot of canopy total SIF_{NIR} summed by three leaf layers (computed with separately controlled $SIFy_{NIR_Ln}$ (**a**) and $LAI_{_Ln}$ (**b**)) against canopy $SIF_{NIR_tot_C}$ calculated from measured SIF_{NIR_C}. Note: $ALSIF_{NIR_L1+L2+L3}$ was canopy total SIF_{NIR} computed with constant $LAI_{_Ln}$ for three leaf layers, $AFSIF_{NIR_L1+L2+L3}$ was canopy total SIF_{NIR} computed with constant $SIFy_{NIR_Ln}$ for three leaf layers.

3.4. Relationships Between Leaf-Layer SIF and Canopy GPP

Using diurnal measurements collected at anthesis and grain filling, we assessed the strength of the relationships between SIF_{NIR} from different leaf layers and canopy GPP (Figure 5). Consistent with the pattern shown in Figure 2, SIF_{NIR_L1} had the strongest correlation with $SIF_{NIR_tot_C}$ ($R^2 = 0.83$), followed by SIF_{NIR_L2} ($R^2 = 0.79$) and SIF_{NIR_L3} ($R^2 = 0.68$). The relationship between $SIF_{NIR_L1+L2+L3}$ and $SIF_{NIR_tot_C}$ yielded an R^2 of 0.84 and an RMSE of 0.62 $mW/m^2/nm/sr$ (Figure 5a–d).

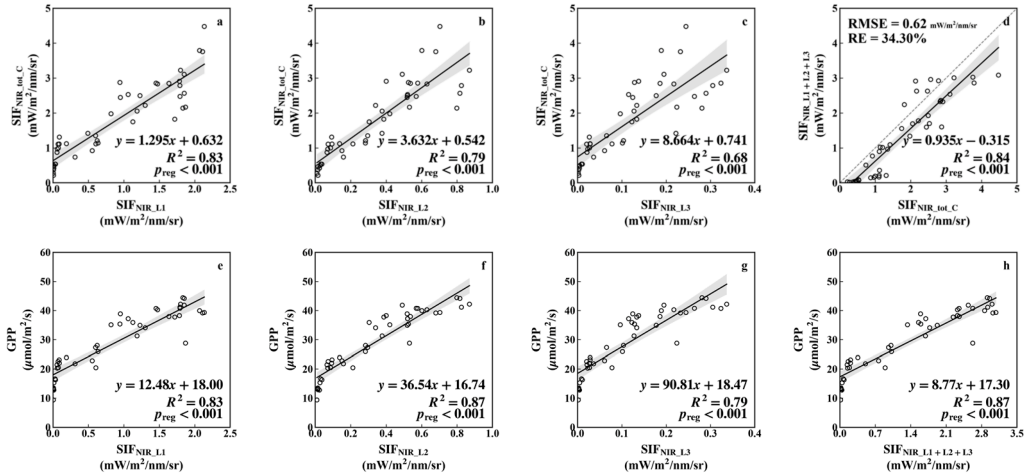


Figure 5. Scatter plots of SIF from individual leaf layers and their three-layer sum against $SIF_{NIR_tot_C}$ (**a**–**d**) and GPP (**e**–**h**) during the flowering and filling stages.

Figure 5e–h shows the relationships between leaf-layer SIFNIR and canopy GPP. Unlike the relationships with canopy SIF_{NIR_tot}, the strongest correlation with GPP was observed for SIF_{NIR_L2} ($R^2 = 0.87$), closely matching that of $SIF_{NIR_L1+L2+L3}$ ($R^2 = 0.87$). SIF_{NIR_L1} and SIF_{NIR_L3} showed weaker correlations, with R^2 values of 0.83 and 0.79, respectively. Calculated $SIF_{NIR_tot_C}$ was less strongly correlated with GPP ($R^2 = 0.81$; Figure 6) than $SIF_{NIR_L1+L2+L3}$.

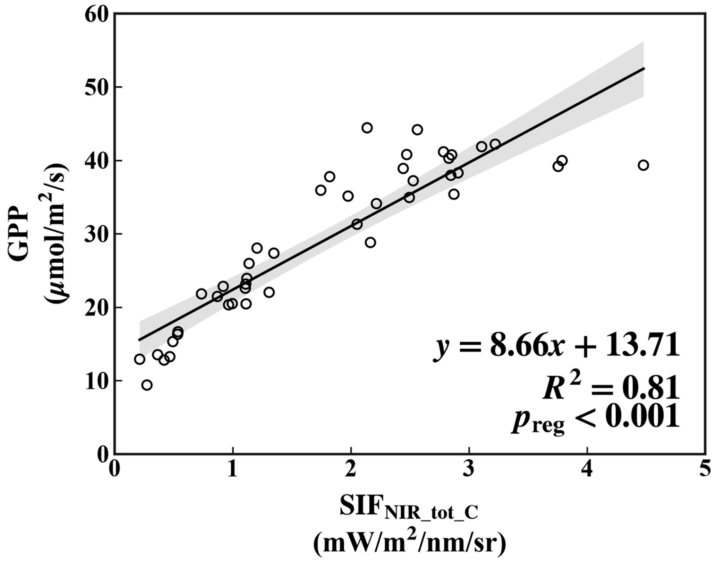


Figure 6. Scatter plot of GPP and $SIF_{NIR_tot_C}$ during the flowering and filling stages.

4. Discussion

4.1. Contributions of SIF from Different Leaf Layers to Canopy SIF

This study showed that SIF_{NIR} from the upper two leaf layers, particularly the first layer, was most strongly correlated with canopy SIF_{NIR}. The first layer also contributed substantially more to total canopy SIF_{NIR} than either of the other two layers (Table 1 and Figure 3). This can be explained by light interception in the first leaf layer, which intercepts most of the incoming photosynthetically active radiation, leaving less radiation available for absorption in the lower canopy. Consequently, lower leaves emit less SIF_{NIR}, and their emissions are strongly influenced by the structure of the overlying first layer. The second and third layers therefore contribute considerably less to canopy SIF than the first layer. Previous studies have also suggested that the growth status of upper-canopy leaves better represents that of the whole canopy. For example, He et al. [41] found that upper leaf layers in rice more accurately reflected overall crop nitrogen status and provided more suitable indicators for nitrogen diagnosis. Fluorescence from shaded leaves in the lower canopy has also been reported to account for only a small fraction of total canopy SIF [42]. These findings support the stronger correlation of upper-layer SIF_{NIR} with canopy SIF_{NIR} and its larger contribution. When canopy measurements are constrained, measurements of LAI and fluorescence associated with D1 leaves, together with estimated APAR for the first leaf layer, could be used to calculate first-layer SIF_{NIR} emissions. These estimates could serve as an auxiliary indicator of changes in canopy SIF.

At anthesis and grain filling, second-layer SIF_{NIR} showed the strongest relationship with canopy GPP among the three leaf layers, closely matching that of the three-layer SIF sum. This pattern may reflect the combined effects of leaf physiological status and the vertical distribution of light. The second layer may occupy an intermediate light environment, with less exposure to high irradiance than the uppermost layer and greater light availability than the third layer. This balance could reduce both high-light saturation of photosynthesis and low-light limitation. Consistent with this interpretation, Zhu et al. [43] found that wheat leaf photosynthesis tended to saturate at high APAR, whereas far-red SIF continued to increase, demonstrating how radiation can modify the SIF–photosynthesis relationship.

The contribution of foliage below the upper canopy also deserves attention. Zhang et al. [44] highlighted the substantial contribution of shaded leaves to canopy GPP and the importance of representing this contribution in productivity models. More recently,

Zhang et al. [45] improved SIF-based GPP estimation by distinguishing sunlit and shaded foliage. Similarly, Zhang et al. [46] found that hemispherical SIF measurements were more strongly related to GPP than nadir measurements. Together, these findings suggest that incorporating fluorescence information from within the canopy may help capture photosynthetic dynamics less well represented by observations dominated by upper-canopy leaves. Given the dependence of canopy fluorescence on viewing geometry [47], multi-angle observations could provide a useful means of exploring the contribution of middle-canopy SIF to GPP estimation.

4.2. Upscaling Leaf-Level SIF to Canopy SIF

This study used a simple approach combining layer-specific APAR constraints, measured SIF_{NIR} emission yields at different leaf positions, and LAI allocation to calculate SIF_{NIR} emissions from individual leaf layers. Emissions from the three layers were summed to obtain canopy $SIF_{NIR_L1+L2+L3}$ and evaluated against canopy SIF_{NIR_tot}. The two estimates were strongly correlated ($R^2 = 0.84$; Figure 2d), supporting the effectiveness of this approach for upscaling leaf-level SIF_{NIR} to the canopy. Canopy SIF integrates multiple influences, including the effects of canopy structure and physiological properties on SIF_{NIR} transfer within the canopy. In the upscaling procedure, leaf SIFy represented leaf physiological information, while LAI represented canopy structure. Measurements of $SIFy_{NIR}$ at multiple leaf positions and canopy LAI allowed us to examine their respective relationships with canopy $SIFy_{NIR}$. Canopy $SIFy_{NIR}$ was moderately related to leaf $SIFy_{NIR}$ ($R^2 = 0.45$; Figure 7a) but more strongly related to LAI ($R^2 = 0.64$; Figure 7b), suggesting a stronger association with canopy structure. Previous studies have shown that $SIFy_{NIR}$ responds more sensitively than canopy structure to the early stages of vegetation stress [48,49], highlighting its value for detecting short-term changes in photosynthesis. Several studies have developed methods to separate structural and physiological information in $SIFy_{NIR_C}$ [23,34,50,51]. These methods account for fluorescence scattering and reabsorption within the canopy, as well as canopy bidirectional reflectance distribution function effects. Nevertheless, the calculated canopy $SIFy_{NIR}$ remained strongly correlated with LAI, with a stronger correlation than that with leaf $SIFy_{NIR}$. Further research is therefore needed to separate the contributions of leaf $SIFy_{NIR}$ and canopy LAI to canopy fluorescence yield.

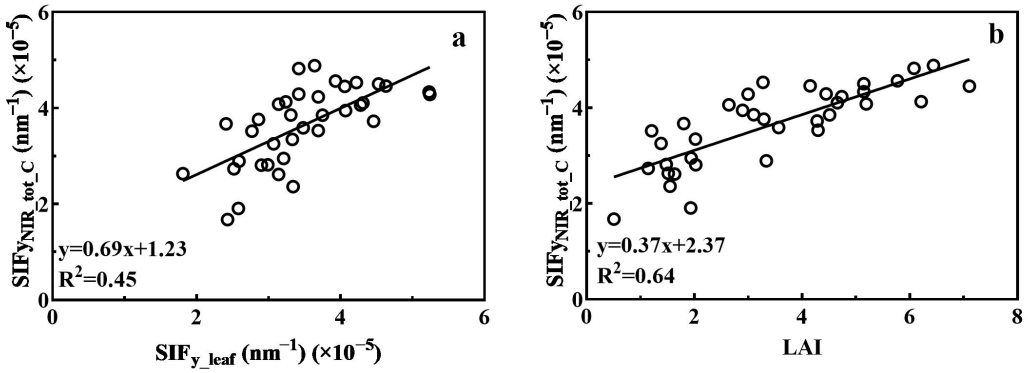


Figure 7. Scatter plot of canopy $SIFy_{NIR_tot_C}$ against leaf-level $SIFy_{NIR_Dn}$ (**a**) and canopy LAI (**b**).

We also assessed the effects of vertical heterogeneity in physiological and structural parameters by retaining or removing variation in SIFy or LAI across leaf layers during the calculations. Omitting vertical variation in leaf layer SIFy reduced the accuracy of canopy SIF_{NIR_tot} estimation, as indicated by a decrease in R^2 and an increase in RMSE. Removing vertical variation in LAI_{Ln} had a greater effect: R^2 decreased from 0.84 to 0.76, and RMSE increased by 28% (Figure 4b). The greater influence of LAI heterogeneity may reflect its

role in weighting leaf-layer contributions and determining APAR distribution within the canopy. Replacing layer-specific LAI with the mean across layers alters the contribution assigned to each layer and may therefore reduce the accuracy of the canopy SIF estimate. This is particularly relevant because the first layer contributed most to canopy SIF, whereas the second and third layers contributed less and were more weakly correlated with canopy SIF (Figure 2b,c). Previous research has also identified canopy structure as a dominant influence on canopy SIF [52], consistent with the greater loss of estimation accuracy when vertical structural variation was omitted.

4.3. Uncertainties

APAR and SIF for individual leaf layers were estimated using a simplified three-layer representation constrained by canopy APAR and LAI. Although this approach focused on physiologically important upper leaves, lower leaves, unexpanded leaves, and green spikes may also contribute to canopy fluorescence, light interception, and photosynthesis, with their relative importance varying across growth stages. Moreover, allocating canopy green LAI among the three sampled leaf positions may implicitly assign green leaf area from other positions to the modeled layers, thereby affecting their estimated APAR and SIF. These simplifications introduce uncertainty into both the three-layer SIF sum and the relative contributions of individual layers.

Within this three-layer representation, the simplified radiation model assumes a uniform extinction coefficient across leaf layers within each observation and represents vertical differences in light attenuation through layer-specific LAI. However, it does not explicitly account for variations in leaf inclination, canopy clumping, or sunlit and shaded foliage. These simplifications may introduce uncertainty into layer-specific APAR estimates and the inferred SIF contributions in heterogeneous wheat canopies. In addition, SIFy was assumed to remain unchanged with light conditions when calculating SIF for each layer, although it can vary with light intensity. This assumption may affect both the estimated SIF of each layer and its contribution to the three-layer total.

Uncertainty also arises from the estimation of GPP. Estimating daytime respiration from nighttime linear temperature–respiration relationships assumes that the nighttime response remains applicable during the day. Light inhibition of respiration may lead to overestimation of daytime respiration and, consequently, GPP [53]. The uncertainty introduced by this extrapolation and its influence on the SIF–GPP relationships were not quantified in the present study.

The observation conditions and temporal coverage also constrain the interpretation of the results. Measurements were collected under clear-sky conditions. Changes in the proportion of direct and diffuse radiation under cloudy conditions may alter within-canopy light distribution and the relationships between leaf-layer SIF and canopy GPP. Furthermore, the comparison of leaf layers to identify the strongest SIF–GPP relationship was limited to one cultivar at anthesis and grain filling. Missing observations during grain filling may affect the characterization of diurnal SIF and GPP patterns. The limited temporal coverage also prevents phenological effects from being reliably separated from weather effects. Additional observations across more days and under different illumination and weather conditions are therefore needed to assess the consistency of these relationships and the applicability of the findings.

The experiment included two wheat cultivars at one site during the 2017–2018 growing season, with only one observed plot for each cultivar and nitrogen combination. Thus, differences among plots could not be clearly attributed to cultivar or nitrogen effects. Measuring several plants or sampling repeatedly within a plot did not provide independent plot replication. Differences in cultivar architecture, nitrogen availability, environmental conditions, and management practices may affect the observed relationships. Further validation using replicated plots across additional growing seasons, locations, cultivars, and growth stages is therefore needed.

5. Conclusions

In this study, the wheat canopy was divided into three leaf layers according to leaf position. We quantified and compared the contributions of leaf-layer SIF_{NIR} to canopy SIF_{NIR_tot}, examined the effects of vertical heterogeneity in SIFy and LAI on canopy SIF, and assessed the quantitative relationships between leaf-layer SIF and canopy GPP. Calculated SIFNIR from all three layers followed seasonal patterns consistent with those of canopy SIF_{NIR_tot}. SIF_{NIR_L1} contributed the largest proportion of the SIF signal (63.51%) and showed the strongest correlation with canopy SIF_{NIR_tot} ($R^2 = 0.83$), followed by SIF_{NIR_L2} (27.49%; $R^2 = 0.69$) and SIF_{NIR_L3} (9%; $R^2 = 0.52$). The three-layer sum, $SIF_{NIR_L1+L2+L3}$, agreed closely with canopy SIF_{NIR_tot} ($R^2 = 0.84$). Vertical heterogeneity in both SIFy and LAI affected canopy SIF_{NIR_tot}, with LAI having the greater influence. SIF_{NIR} from all three layers was strongly correlated with GPP. The strongest relationship was observed for SIF_{NIR_L2} ($R^2 = 0.87$), matching that of $SIF_{NIR_L1+L2+L3}$, followed by SIF_{NIR_L1} ($R^2 = 0.83$) and SIF_{NIR_L3} ($R^2 = 0.79$). These findings, based on a simplified three-layer canopy representation and a single-site, single-season experiment without independent plot replication, require validation under broader wheat-growing conditions. Future work could further examine middle-canopy contributions to GPP and use multi-angle SIF observations to capture information from middle and lower canopy layers, potentially improving SIF-based estimates of crop productivity. Vertical canopy heterogeneity should also be explicitly considered in canopy SIF simulations.

Author Contributions: Conceptualization, J.Z. and X.Y.; methodology, software, validation, formal analysis, investigation, and visualization, J.Z.; data curation, J.Z., R.H., X.X., Y.H., W.L. and Y.G.; resources, X.Y.; writing—original draft preparation, J.Z., R.H., X.X., Y.H., W.L., Y.G., L.L., H.Z., C.J., T.C., Y.T., Y.Z., W.C. and X.Y.; writing—review and editing, J.Z., R.H., X.X., Y.H., W.L., Y.G. and X.Y.; supervision, R.H., L.L., H.Z., C.J., T.C., Y.T., Y.Z., W.C. and X.Y.; project administration and funding acquisition, X.Y. All authors have read and agreed to the published version of the manuscript.

Funding: This work was supported by the National major agricultural science and technology projects (0305), Natural Science Fund of Jiangsu Province (BK20251555), the National Natural Science Foundation of China (42601701, 32471996), Research and Development of Precision Crop Phenotyping and Key Equipment for Breeding Fields (QTPY2026023), the Jiangsu Funding Program for Excellent Postdoctoral Talent (2024ZB174), the Fellowship of China Postdoctoral Science Foundation (2024M751438).

Data Availability Statement: The data supporting the findings of this study are available from the corresponding author, Xia Yao, upon reasonable request.

Acknowledgments: During the preparation of this manuscript, the authors used ChatGPT (GPT-6 Astra, OpenAI) to assist with translation from Chinese into English. The authors reviewed and edited the translated text and take full responsibility for the content of this publication.

Conflicts of Interest: The authors declare no conflicts of interest.

Abbreviations

The following abbreviations are used in this manuscript:

SIF	Solar-induced chlorophyll fluorescence
SIFy	SIF emission yield
NIR	Near-infrared
GPP	Gross primary productivity
LAI	Leaf area index
Cab	Chlorophyll a and b content
PAR	Photosynthetically active radiation
APAR	Absorbed photosynthetically active radiation
fAPAR	Fraction of absorbed photosynthetically active radiation
DOY	Day of year
LT	Local time
PPFD	Photosynthetic photon flux density
aFSR	Advanced fluorescence spectrum reconstruction
NDVI	Normalized difference vegetation index
NIRv	Near-infrared reflectance of vegetation
RTM	Radiative transfer model
RMSE	Root mean square error
RE	Relative error
SIF_{NIR_C}	Near-infrared solar-induced chlorophyll fluorescence at 761 nm at canopy scale
$SIFy_{NIR_C}$	Near-infrared SIF emission yield at canopy scale
$SIF_{NIR_tot_C}$	Total near-infrared SIF emission at the photosystem level estimated from canopy SIF_{NIR}
$SIFy_{NIR_tot_C}$	Total near-infrared SIF emission yield at the photosystem level estimated from canopy SIF_{NIR}
Dn, Ln	The nth leaf position and its corresponding leaf layer, respectively
SIF_{NIR_Ln}	Near-infrared SIF emission from the nth leaf layer
$SIFy_{NIR_Ln}$	Near-infrared SIF emission yield assigned to the nth leaf layer
$SIFy_{NIR_Dn}$	Leaf-level near-infrared SIF emission yield measured at the nth leaf position
$SIF_{NIR_L1+L2+L3}$	Sum of near-infrared SIF emissions from the three leaf layers
$ALSIF_{NIR_L1+L2+L3}$	Three-layer sum of near-infrared SIF calculated with LAI set to the mean across layers
$AFSIF_{NIR_L1+L2+L3}$	Three-layer sum of near-infrared SIF calculated with SIF yield set to the mean across layers
$fAPAR_{Dn}$	Fraction of photosynthetically active radiation absorbed at the leaf scale
$fAPAR_c$	Fraction of photosynthetically active radiation absorbed by the canopy
$APAR_c$	Photosynthetically active radiation absorbed by the canopy
$APAR_{Ln}$	Photosynthetically active radiation absorbed by the nth leaf layer
PAR_{in}	Incoming photosynthetically active radiation
PAR_{in_Ln}	Photosynthetically active radiation entering the nth leaf layer
$PAR_{in_L(n+1)}$	Photosynthetically active radiation reaching the next leaf layer
R_{Dn}	Leaf reflectance
TM_{Dn}	Leaf transmittance
R_λ	Canopy reflectance at wavelength λ
L_λ	Canopy spectral radiance at wavelength λ
I_λ	Reference-panel spectral radiance at wavelength λ
R_{NIR}	Near-infrared reflectance
fesc	Escape fraction of near-infrared SIF
k	Light extinction coefficient
λ	Wavelength
Pn	Canopy net photosynthetic rate
Rn	Canopy respiration rate
R^2	Coefficient of determination

Appendix A

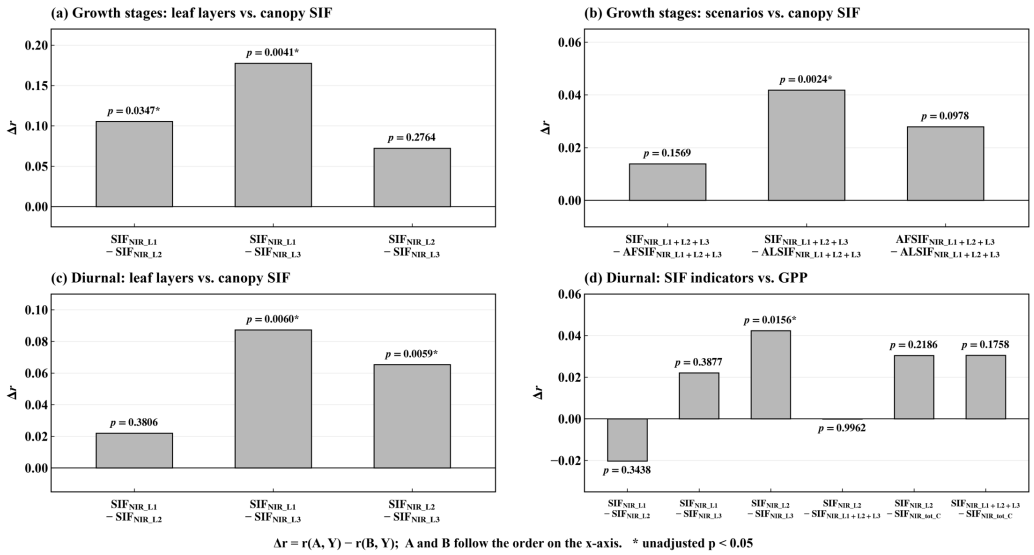


Figure A1. Differences in Pearson correlations between SIF indicators. (**a**) Leaf-layer comparisons across growth stages; (**b**) comparisons of the three-layer sum with uniform-SIF-yield (AF) and uniform-LAI (AL) scenarios; (**c**) diurnal leaf-layer comparisons; and (**d**) diurnal SIF-indicator comparisons with GPP. $\Delta r = r(A, Y) - r(B, Y)$, with A and B ordered as on the *x*-axis. Y is canopy SIF in (**a**–**c**) and GPP in (**d**). Labels show two-sided Williams-test *p* values; * indicates $p < 0.05$.

References

1. Hu, P.; Tu, F.; Li, S.; Pan, Y.; Kong, C.; Zhang, X.; Wang, S.; Sun, Y.; Qiu, D.; Wu, L.; et al. Low-Cd wheat varieties and soil Cd safety thresholds for local soil health management in south Jiangsu province, east China. *Agric. Ecosyst. Environ.* **2023**, *341*, 108211. [CrossRef]
2. Liu, L.; Liu, X.; Hu, J.; Guan, L. Assessing the wavelength-dependent ability of solar-induced chlorophyll fluorescence to estimate the GPP of winter wheat at the canopy level. *Int. J. Remote Sens.* **2017**, *38*, 4396–4417. [CrossRef]
3. Liu, Z.; Zhao, F.; Liu, X.; Yu, Q.; Wang, Y.; Peng, X.; Cai, H.; Lu, X. Direct estimation of photosynthetic CO2 assimilation from solar-induced chlorophyll fluorescence (SIF). *Remote Sens. Environ.* **2022**, *271*, 112893. [CrossRef]
4. Shen, Q.; Lin, J.; Yang, J.; Zhao, W.; Wu, J. Exploring the Potential of Spatially Downscaled Solar-Induced Chlorophyll Fluorescence to Monitor Drought Effects on Gross Primary Production in Winter Wheat. *IEEE J. Sel. Top. Appl. Earth Obs. Remote Sens.* **2022**, *15*, 2012–2022. [CrossRef]
5. Zhang, Q.; Chen, J.M.; Ju, W.; Zhang, Y.; Li, Z.; He, L.; Pacheco-Labrador, J.; Li, J.; Qiu, B.; Zhang, X.; et al. Ground-Based Multiangle Solar-Induced Chlorophyll Fluorescence Observation and Angular Normalization for Assessing Crop Productivity. *J. Geophys. Res. Biogeosci.* **2021**, *126*, e2020JG006082. [CrossRef]
6. Chen, R.; Liu, L.; Liu, X. Leaf chlorophyll contents dominates the seasonal dynamics of SIF/GPP ratio: Evidence from continuous measurements in a maize field. *Agric. For. Meteorol.* **2022**, *323*, 109070. [CrossRef]
7. Li, Z.H.; Zhang, Q.; Li, J.; Yang, X.; Wu, Y.F.; Zhang, Z.Y.; Wang, S.H.; Wang, H.Z.; Zhang, Y.G. Solar-induced chlorophyll fluorescence and its link to canopy photosynthesis in maize from continuous ground measurements. *Remote Sens. Environ.* **2020**, *236*, 111420. [CrossRef]
8. Lu, X.; Liu, Z.; Zhao, F.; Tang, J. Comparison of total emitted solar-induced chlorophyll fluorescence (SIF) and top-of-canopy (TOC) SIF in estimating photosynthesis. *Remote Sens. Environ.* **2020**, *251*, 112083. [CrossRef]
9. Zhang, Z.; Zhang, Y.; Porcar-Castell, A.; Joiner, J.; Guanter, L.; Yang, X.; Migliavacca, M.; Ju, W.; Sun, Z.; Chen, S.; et al. Reduction of structural impacts and distinction of photosynthetic pathways in a global estimation of GPP from space-borne solar-induced chlorophyll fluorescence. *Remote Sens. Environ.* **2020**, *240*, 111722. [CrossRef]
10. Drecer, M. Dynamics of vertical leaf nitrogen distribution in a vegetative wheat canopy. Impact on canopy photosynthesis. *Ann. Bot.* **2000**, *86*, 821–831. [CrossRef]

11. Li, H.; Zhao, C.; Yang, G.; Feng, H. Variations in crop variables within wheat canopies and responses of canopy spectral characteristics and derived vegetation indices to different vertical leaf layers and spikes. *Remote Sens. Environ.* **2015**, *169*, 358–374. [CrossRef]
12. Wu, B.; Huang, W.; Ye, H.; Luo, P.; Ren, Y.; Kong, W. Using multi-angular hyperspectral data to estimate the vertical distribution of leaf chlorophyll content in wheat. *Remote Sens.* **2021**, *13*, 1501. [CrossRef]
13. Xiong, S.-P.; Cao, W.-B.; Cao, R.; Zhang, Z.-Y.; Fu, X.-L.; Xu, S.-J.; Pan, H.-Q.; Wang, X.-C.; Ma, X.-M. Effects of horizontal structure on canopy vertical structure, microenvironment and yield of Triticum aestivum. *Chin. J. Plant Ecol.* **2022**, *46*, 188–196. [CrossRef]
14. Migliavacca, M.; Perez-Priego, O.; Rossini, M.; El-Madany, T.S.; Moreno, G.; van der Tol, C.; Rascher, U.; Berninger, A.; Bessenbacher, V.; Burkart, A.; et al. Plant functional traits and canopy structure control the relationship between photosynthetic CO2 uptake and far-red sun-induced fluorescence in a Mediterranean grassland under different nutrient availability. *New Phytol.* **2017**, *214*, 1078–1091. [CrossRef] [PubMed]
15. Wu, G.; Jiang, C.; Kimm, H.; Wang, S.; Bernacchi, C.; Moore, C.E.; Suyker, A.; Yang, X.; Magney, T.; Frankenberg, C.; et al. Difference in seasonal peak timing of soybean far-red SIF and GPP explained by canopy structure and chlorophyll content. *Remote Sens. Environ.* **2022**, *279*, 113104. [CrossRef]
16. Gitelson, A.A.; Peng, Y.; Huemmrich, K.F. Relationship between fraction of radiation absorbed by photosynthesizing maize and soybean canopies and NDVI from remotely sensed data taken at close range and from MODIS 250m resolution data. *Remote Sens. Environ.* **2014**, *147*, 108–120. [CrossRef]
17. Zhao, C.; Li, H.; Li, P.; Yang, G.; Gu, X.; Lan, Y. Effect of Vertical Distribution of Crop Structure and Biochemical Parameters of Winter Wheat on Canopy Reflectance Characteristics and Spectral Indices. *IEEE Trans. Geosci. Remote Sens.* **2017**, *55*, 236–247. [CrossRef]
18. Yang, P.; Verhoef, W.; van der Tol, C. The mSCOPE model: A simple adaptation to the SCOPE model to describe reflectance, fluorescence and photosynthesis of vertically heterogeneous canopies. *Remote Sens. Environ.* **2017**, *201*, 1–11. [CrossRef]
19. Hornero, A.; North, P.R.J.; Zarco-Tejada, P.J.; Rascher, U.; Martín, M.P.; Migliavacca, M.; Hernandez-Clemente, R. Assessing the contribution of understory sun-induced chlorophyll fluorescence through 3-D radiative transfer modelling and field data. *Remote Sens. Environ.* **2021**, *253*, 112195. [CrossRef]
20. Regaieg, O.; Yin, T.; Malenovský, Z.; Cook, B.D.; Morton, D.C.; Gastellu-Etchegorry, J.-P. Assessing impacts of canopy 3D structure on chlorophyll fluorescence radiance and radiative budget of deciduous forest stands using DART. *Remote Sens. Environ.* **2021**, *265*, 112673. [CrossRef]
21. Gao, S.; Huete, A.; Kobayashi, H.; Doody, T.M.; Liu, W.; Wang, Y.; Zhang, Y.; Lu, X. Simulation of solar-induced chlorophyll fluorescence in a heterogeneous forest using 3-D radiative transfer modelling and airborne LiDAR. *ISPRS J. Photogramm. Remote Sens.* **2022**, *191*, 1–17. [CrossRef]
22. Liu, X.; Guanter, L.; Liu, L.; Damm, A.; Malenovský, Z.; Rascher, U.; Peng, D.; Du, S.; Gastellu-Etchegorry, J.-P. Downscaling of solar-induced chlorophyll fluorescence from canopy level to photosystem level using a random forest model. *Remote Sens. Environ.* **2019**, *231*, 110772. [CrossRef]
23. Yang, P.; van der Tol, C.; Campbell, P.K.E.; Middleton, E.M. Fluorescence Correction Vegetation Index (FCVI): A physically based reflectance index to separate physiological and non-physiological information in far-red sun-induced chlorophyll fluorescence. *Remote Sens. Environ.* **2020**, *240*, 111676. [CrossRef]
24. Zeng, Y.L.; Badgley, G.; Dechant, B.; Ryu, Y.; Chen, M.; Berry, J.A. A practical approach for estimating the escape ratio of near-infrared solar-induced chlorophyll fluorescence. *Remote Sens. Environ.* **2019**, *232*, 111209. [CrossRef]
25. Morozumi, T.; Kato, T.; Kobayashi, H.; Sakai, Y.; Nakashima, N.; Buareal, K.; Nasahara, K.N.; Akitsu, T.K.; Murayama, S.; Noda, H.M.; et al. Contributions of the understory and midstory to total canopy solar-induced chlorophyll fluorescence in a ground-based study in conjunction with seasonal gross primary productivity in a cool-temperate deciduous broadleaf forest. *Remote Sens. Environ.* **2023**, *284*, 113340. [CrossRef]
26. Zhu, K.; Chen, J.; Wang, S.; Fang, H.; Chen, B.; Zhang, L.; Li, Y.; Zheng, C.; Amir, M. Characterization of the layered SIF distribution through hyperspectral observation and SCOPE modeling for a subtropical evergreen forest. *ISPRS J. Photogramm. Remote Sens.* **2023**, *201*, 78–91. [CrossRef]
27. El Wazziki, H.; El Yousfi, B.; Serghat, S. Contributions of three upper leaves of wheat, either healthy or inoculated by Bipolaris sorokiniana, to yield and yield components. *Aust. J. Crop Sci.* **2015**, *9*, 629–637.
28. Jiang, N.; Di, Y.T.; Xu, K.Z.; Zhao, G.C.; Ling, F.L.; Wu, Z.H.; Zhang, Z.A. Changes of photosynthetic characteristics in top three leaves of rice (*Oryza sativa* L.) cultivars released in different years in Jilin Province. *Acta Agron. Sin.* **2011**, *37*, 703–710. [CrossRef]
29. Song, Q.; Xiao, H.; Xiao, X.; Zhu, X.-G. A new canopy photosynthesis and transpiration measurement system (CAPTS) for canopy gas exchange research. *Agric. For. Meteorol.* **2016**, *217*, 101–107. [CrossRef]

30. Mõttus, M.; Hernandez-Clemente, R.; Perheentupa, V.; Markiet, V.; Aalto, J.; Bäck, J.; Nichol, C.J. Measurement of diurnal variation in needle PRI and shoot photosynthesis in a boreal forest. *Remote Sens.* **2018**, *10*, 1019. [CrossRef]
31. Jia, M.; Zhu, J.; Ma, C.; Alonso, L.; Li, D.; Cheng, T.; Tian, Y.; Zhu, Y.; Yao, X.; Cao, W. Difference and potential of the upward and downward sun-induced chlorophyll fluorescence on detecting leaf nitrogen concentration in wheat. *Remote Sens.* **2018**, *10*, 1315. [CrossRef]
32. Köppl, C.J.; Malureanu, R.; Dam-Hansen, C.; Wang, S.; Jin, H.; Barchiesi, S.; Serrano Sandí, J.M.; Muñoz-Carpena, R.; Johnson, M.; Durán-Quesada, A.M.; et al. Hyperspectral reflectance measurements from UAS under intermittent clouds: Correcting irradiance measurements for sensor tilt. *Remote Sens. Environ.* **2021**, *267*, 112719. [CrossRef]
33. Viña, A.; Gitelson, A.A. New developments in the remote estimation of the fraction of absorbed photosynthetically active radiation in crops. *Geophys. Res. Lett.* **2005**, *32*, L17403. [CrossRef]
34. Yang, P.Q.; van der Tol, C.; Campbell, P.K.E.; Middleton, E.M. Unraveling the physical and physiological basis for the solar-induced chlorophyll fluorescence and photosynthesis relationship using continuous leaf and canopy measurements of a corn crop. *Biogeosciences* **2021**, *18*, 441–465. [CrossRef]
35. Zhao, F.; Li, R.; Verhoef, W.; Cogliati, S.; Liu, X.; Huang, Y.; Guo, Y.; Huang, J. Reconstruction of the full spectrum of solar-induced chlorophyll fluorescence: Intercomparison study for a novel method. *Remote Sens. Environ.* **2018**, *219*, 233–246. [CrossRef]
36. Badgley, G.; Field, C.B.; Berry, J.A. Canopy near-infrared reflectance and terrestrial photosynthesis. *Sci. Adv.* **2017**, *3*, e1602244. [CrossRef]
37. Rouse, J.W., Jr.; Haas, R.H.; Schell, J.A.; Deering, D.W. Monitoring vegetation systems in the Great Plains with ERTS. In *Proceedings of the Third Earth Resources Technology Satellite-1 Symposium*; NASA: Washington, DC, USA, 1974; Volume 1, pp. 309–317.
38. Chang, C.Y.; Wen, J.; Han, J.; Kira, O.; LeVonne, J.; Melkonian, J.; Riha, S.J.; Skovira, J.; Ng, S.; Gu, L.; et al. Unpacking the drivers of diurnal dynamics of sun-induced chlorophyll fluorescence (SIF): Canopy structure, plant physiology, instrument configuration and retrieval methods. *Remote Sens. Environ.* **2021**, *265*, 112672. [CrossRef]
39. Gu, L.; Han, J.; Wood, J.D.; Chang, C.Y.; Sun, Y. Sun-induced Chl fluorescence and its importance for biophysical modeling of photosynthesis based on light reactions. *New Phytol.* **2019**, *223*, 1179–1191. [CrossRef] [PubMed]
40. Diedenhofen, B.; Musch, J. cocor: A comprehensive solution for the statistical comparison of correlations. *PLoS ONE* **2015**, *10*, e0121945. [CrossRef]
41. He, J.; Ma, J.; Cao, Q.; Wang, X.; Yao, X.; Cheng, T.; Zhu, Y.; Cao, W.; Tian, Y. Development of critical nitrogen dilution curves for different leaf layers within the rice canopy. *Eur. J. Agron.* **2022**, *132*, 126414. [CrossRef]
42. Zhang, Z.; Zhang, Y.; Zhang, Q.; Chen, J.M.; Porcar-Castell, A.; Guanter, L.; Wu, Y.; Zhang, X.; Wang, H.; Ding, D.; et al. Assessing bi-directional effects on the diurnal cycle of measured solar-induced chlorophyll fluorescence in crop canopies. *Agric. For. Meteorol.* **2020**, *295*, 108147. [CrossRef]
43. Zhu, J.; Lu, J.; Xu, X.; Huang, Y.; Li, W.; Gu, Y.; Zheng, H.; Jiang, C.; Cheng, T.; Tian, Y.; et al. Estimating leaf net photosynthetic rate in wheat using sun-induced chlorophyll fluorescence. *Smart Agric. Technol.* **2026**, *15*, 102444. [CrossRef]
44. Zhang, F.; Chen, J.M.; Chen, J.; Gough, C.M.; Martin, T.A.; Dragoni, D. Evaluating spatial and temporal patterns of MODIS GPP over the conterminous U.S. against flux measurements and a process model. *Remote Sens. Environ.* **2012**, *124*, 717–729. [CrossRef]
45. Zhang, Z.; Chen, J.M.; Zhang, Y.; Li, M. Improving the ability of solar-induced chlorophyll fluorescence to track gross primary production through differentiating sunlit and shaded leaves. *Agric. For. Meteorol.* **2023**, *341*, 109658. [CrossRef]
46. Zhang, Z.; Zhang, X.; Porcar-Castell, A.; Chen, J.M.; Ju, W.; Wu, L.; Wu, Y.; Zhang, Y. Sun-induced chlorophyll fluorescence is more strongly related to photosynthesis with hemispherical than nadir measurements: Evidence from field observations and model simulations. *Remote Sens. Environ.* **2022**, *279*, 113118. [CrossRef]
47. He, Y.; Zeng, Y.; Hao, D.; Shabanov, N.V.; Huang, J.; Yin, G.; Biriukova, K.; Lu, W.; Gao, Y.; Celesti, M.; et al. Combining geometric-optical and spectral invariants theories for modeling canopy fluorescence anisotropy. *Remote Sens. Environ.* **2025**, *323*, 114716. [CrossRef]
48. Wang, N.; Yang, P.; Clevers, J.G.P.W.; Wieneke, S.; Kooistra, L. Decoupling physiological and non-physiological responses of sugar beet to water stress from sun-induced chlorophyll fluorescence. *Remote Sens. Environ.* **2023**, *286*, 113445. [CrossRef]
49. Wu, L.; Zhang, X.; Rossini, M.; Wu, Y.; Zhang, Z.; Zhang, Y. Physiological dynamics dominate the response of canopy far-red solar-induced fluorescence to herbicide treatment. *Agric. For. Meteorol.* **2022**, *323*, 109063. [CrossRef]
50. Regaieg, O.; Malenovský, Z.; Siegmann, B.; Buffat, J.; Krämer, J.; Lauret, N.; Le Dantec, V. DART-based temporal and spatial retrievals of solar-induced chlorophyll fluorescence quantum efficiency from in-situ and airborne crop observations. *Remote Sens. Environ.* **2025**, *319*, 114636. [CrossRef]
51. Zeng, Y.; Chen, M.; Hao, D.; Damm, A.; Badgley, G.; Rascher, U.; Johnson, J.E.; Dechant, B.; Siegmann, B.; Ryu, Y.; et al. Combining near-infrared radiance of vegetation and fluorescence spectroscopy to detect effects of abiotic changes and stresses. *Remote Sens. Environ.* **2022**, *270*, 112856. [CrossRef]

52. Dechant, B.; Ryu, Y.; Badgley, G.; Zeng, Y.; Berry, J.A.; Zhang, Y.G.; Goulas, Y.; Li, Z.H.; Zhang, Q.; Kang, M.; et al. Canopy structure explains the relationship between photosynthesis and sun-induced chlorophyll fluorescence in crops. *Remote Sens. Environ.* **2020**, *241*, 111733. [CrossRef]
53. Cai, T.; Flanagan, L.B.; Syed, K.H. Warmer and drier conditions stimulate respiration more than photosynthesis in a boreal peatland ecosystem: Analysis of automatic chambers and eddy covariance measurements. *Plant Cell Environ.* **2010**, *33*, 394–407. [CrossRef]

Disclaimer/Publisher's Note: The statements, opinions and data contained in all publications are solely those of the individual author(s) and contributor(s) and not of MDPI and/or the editor(s). MDPI and/or the editor(s) disclaim responsibility for any injury to people or property resulting from any ideas, methods, instructions or products referred to in the content.